Published November 4, 2020, doi:10.4049/jimmunol.2000848

A Novel Fusion of IL-10 Engineered to Traffic across Intestinal Epithelium to Treat Colitis

Nicole C. Fay,* Baby-Periyanayaki Muthusamy,* Linh P. Nyugen,* Radhika C. Desai,* Alistair Taverner,† Julia MacKay,† Minji Seung,* Tom Hunter,* Keyi Liu,* Apurva Chandalia,* Michael P. Coyle,* Hyojin L. Kim,* Sally Postlethwaite,* Khushdeep Mangat,* Lisa Song,* Elbert Seto,* Aatif Alam,* Charles V. Olson,* Weijun Feng,* Maziyar Saberi,* Tahir A. Mahmood,* and Randall J. Mrsny*,†

IL-10 is a potent anti-inflammatory cytokine capable of suppressing a number of proinflammatory signals associated with intestinal inflammatory diseases, such as ulcerative colitis and Crohn's disease. Clinical use of human IL-10 (hIL-10) has been limited by anemia and thrombocytopenia following systemic injection, side effects that might be eliminated by a gut-restricted distribution. We have identified a transcytosis pathway used by cholix, an exotoxin secreted by nonpandemic forms of the intestinal pathogen *Vibrio cholerae*. A nontoxic fragment of the first 386 aa of cholix was genetically fused to hIL-10 to produce recombinant AMT-101. In vitro and in vivo characterization of AMT-101 showed it to efficiently cross healthy human intestinal epithelium (SMI-100) by a vesicular transcytosis process, activate hIL-10 receptors in an engineered U2OS osteosarcoma cell line, and increase cellular phospho-STAT3 levels in J774.2 mouse macrophage cells. AMT-101 was taken up by inflamed intestinal mucosa and activated pSTAT3 in the lamina propria with limited systemic distribution. AMT-101 administered to healthy mice by oral gavage or to cynomolgus monkeys (nonhuman primates) by colonic spray increased circulating levels of IL-1R antagonist (IL-1Ra). Oral gavage of AMT-101 in two mouse models of induced colitis prevented associated pathological events and plasma cytokine changes. Overall, these studies suggest that AMT-101 can efficiently overcome the epithelial barrier to focus biologically active IL-10 to the intestinal lamina propria. *The Journal of Immunology*, **2020, 205: 000–000.**

Interleukin-10 functions as a key immunoregulatory cytokine in the intestine and is considered to be a central anti-inflammatory element in regulating the human immune response to a plethora of proinflammatory mediators (1–3). Knockout of IL-10 expression in mice results in their predisposition toward intestinal inflammation in response to environmental cues: outcomes corrected by systemic administration of exogenous IL-10 (4). Newborns lacking the ability to express functional IL-10 similarly demonstrate severe intestinal inflammation soon after birth, and defects in the IL-10 signaling pathway increase the risk of pediatric inflammatory bowel disease (IBD) (5, 6). Examination of individuals with Crohn's disease and ulcerative colitis highlighted polymorphisms in the IL-10 gene promoter region and reduced serum IL-10 levels that correlated with IBD (5, 7–9). Macrophages within the intestinal lamina propria have been identified as a significant source for IL-10 involved in epithelial wound closure through activation of specific pro-proliferative pathways (10). Thus, IL-10 functions as a master regulator of intestinal mucosal homeostasis, making it a promising therapeutic agent for managing the clinical symptoms associated with IBD (11).

Despite multiple preclinical studies supporting the promise of human IL-10 (hIL-10) to correct IBD-like symptoms induced in various animal models that exhibit strong correlations with intestinal inflammation, clinical studies to treat IBD with this cytokine have had disappointing outcomes, primarily because of dose-limiting side effects following systemic administration (12–14). Five potential explanations have been put forth to explain the lack of clinical efficacy of hIL-10 treatment as a strategy for treating IBD: 1) hIL-10 dose was too low to achieve local intestinal exposure required to elicit a response, 2) excessive interpatient variability in responses, 3) hIL-10 can only have clinical benefit for preventing and not correcting disease, 4) hIL-10 alone is insufficient to suppress all the proinflammatory pathways engaged in patients with chronic disease, and/or 5) the immunostimulatory actions of hIL-10 counterbalanced its immunosuppressive properties (15). Several of these proposed reasons could be associated with the systemic rather than intestinal-directed actions of hIL-10 in these studies, with dose-limiting side effects of decreased hemoglobin and thrombocyte counts being the most significant (13, 14). Further, efforts to achieve efficacious hIL-10 levels in the intestinal lamina propria through higher systemic dosing

*Applied Molecular Transport, South San Francisco, CA 94080; and †Department of Pharmacy and Pharmacology, University of Bath, BA2 7AY Bath, United Kingdom

ORCIDs: 0000-0001-5305-8466 (N.C.F.); 0000-0001-6704-9579 (B.-P.M.); 0000-0002-2507-8694 (A.T.); 0000-0003-0864-8744 (K.L.); 0000-0003-1847-2236 (M.P.C.); 0000-0003-2164-5919 (H.L.K.); 0000-0003-0419-3308 (K.M.); 0000-0003-0803-2827 (E.S.); 0000-0002-1041-2418 (W.F.); 0000-0003-1890-6663 (T.A.M.); 0000-0001-8505-8516 (R.J.M.).

Received for publication July 22, 2020. Accepted for publication October 3, 2020.

Address correspondence and reprint requests to Randall J. Mrsny, University of Bath, Claverton Down, BA2 7AY Bath, U.K. E-mail address: rjm37@bath.ac.uk

The online version of this article contains supplemental material.

Abbreviations used in this article: 5-ASA, 5-aminosalicylic acid; Chx, cholix; Chx386, first 386 aa of Chx; DSS, dextran sulfate sodium; GS, glycine and serine; hGH, human growth hormone; hIL-10, human IL-10; IBD, inflammatory bowel disease; ILI, intraluminal injection; IL-1Ra, IL-1R antagonist; LMAN1, lectin, mannose binding 1; MSD, Meso Scale Discovery; NHP, nonhuman primate; Oxa, oxazolone; PBST, PBS with Tween 20; PK, pharmacokinetics; rhIL-10, recombinant hIL-10; RT, room temperature.

may have induced pro- rather than anti-inflammatory systemic events, such as induction of IFN-γ (4, 15). Thus, it has been suggested that restricting hIL-10 to the intestinal lamina propria may improve its efficacy by reducing its potential for dose-limiting systemic actions (15). This hypothesis is supported by recent studies demonstrating that IL-10 production and basal release by intestinal epithelial cells drive the secretion of additional IL-10 to establish a local, immunosuppressive state that is critical for the regulation of intestinal inflammation (16).

We have examined the feasibility of using a nontoxic fragment of the exotoxin cholix (Chx), using the first 386 aa of Chx (Chx386), to ferry hIL-10 across intestinal epithelial cells via a transcytosis pathway, delivering it to the underlying lamina propria. Chx, a member of the AB family of toxins, is secreted by nonpandemic strains of *Vibrio cholera* as a single chain of amino acids that folds into a three-domain organization (17). The proximal half of Chx hijacks host cell vesicular trafficking elements to facilitate the efficient transcytosis, delivering intact toxin to cells within the underlying lamina propria; a different trafficking mechanism occurs within the lamina propria that allows the latter half of Chx to escape vesicular structures to reach the cytoplasm of these nonpolarized cells, where it enzymatically blocks protein synthesis (18). We have recently demonstrated that the proximal portion of Chx is capable of efficiently delivering a conjoined protein that replaces the latter (toxic) half of the protein to the intestinal lamina propria following oral administration (19). To focus an IL-10 payload to the intestinal lamina propria, a genetic fusion gene of Chx386 and hIL-10 with a glycine–serine-type linker was prepared (20). The resulting chimera, termed AMT-101, was designed through modeling to limit conflicts to facilitate folding of the Chx386 domain as well as folding and dimerization of the hIL-10 monomer elements (17, 21, 22). In this study, we describe AMT-101's functional properties in vitro and in vivo, including its capacity for transcytosis of the intestinal epithelium and specific cellular targeting within the lamina propria, as well as its biological actions in the settings of induced intestinal inflammation and in noninflamed tissues.

Materials and Methods

Expression and purification of Chx386–hIL-10 (AMT-101)

The Chx386–hIL-10 fusion protein was codon optimized for *Escherichia coli* expression. The synthesized gene was cloned into the vector pET-26b (+) DNA expression vector and transformed into *E. coli* BL21(DE3) cells that were cultured by fed-batch fermentation in a stirred tank bioreactor using a defined culture media (23). The culture was induced with 1 mM isopropyl β-D-thiogalactoside, and the temperature was reduced to 26°C. Cultures were continued for a further 12 h after induction before cells were harvested by centrifugation. *E. coli* cell pellets were suspended in double-distilled water and lysed using two passes of high pressure using a microfluidizer. Lysates were clarified by centrifugation, and the inclusion body pellets washed once with 50 mM Tris (pH 8.5), 0.5 M NaCl, and 20 mM EDTA and once with double-distilled water. The product containing inclusion bodies was then solubilized in guanidine HCl and clarified by centrifugation. Solubilized inclusion bodies were diluted into refolding buffer and gently mixed overnight to allow protein refolding. The refolded protein was concentrated, buffer exchanged by ultrafiltration/diafiltration into 25 mM Tris (pH 7.5) and 150 mM NaCl buffer loaded on a Capto Q ImpRes anion exchange column, and then eluted using an NaCl gradient. A polishing step using ceramic hydroxyapatite type I chromatography and an increasing linear sodium phosphate gradient was used to achieve further purification. Final protein concentration was assessed using A_{280}, endotoxin was measured using Charles River Endosafe PTS reader, and purity (>90%) was assessed using size-exclusion HPLC as well as SDS-PAGE.

Western blotting

Samples were separated by electrophoresis in a 4–12% NuPAGE gel (Bio-Rad Laboratories) with m.w. standards (Bio-Rad Laboratories or GE Amersham) prior to transfer onto a polyvinylidene difluoride membrane (Bio-Rad Laboratories) that was probed using a goat polyclonal Ab recognizing hIL-10 (1:1000 dilution, AF-217-NA; R&D Systems) and detected using an alkaline phosphatase–conjugated secondary rabbit anti-goat Ab (1:10,000 dilution, ab6742; Abcam). Protein bands were visualized using an alkaline phosphatase Western blotting substrate (Promega). Recombinant hIL-10 (rhIL-10) was obtained from Enzo Life Sciences (Farmingdale, NY).

IL-10R dimerization

The PathHunter U2OS IL-10R1/IL-10R2 Dimerization Cell Line was obtained from Eurofins (Fremont, CA). In these engineered cells, IL-10 binding to its receptor dimers engages the fusion of β-galactosidase subunits that are linked to IL-10R1 and IL-10R2, thus forming a functional enzyme that serves as a surrogate measure of IL-10 binding to its cognate receptor. Cells were seeded in cell-plating media (100 μl/well of 96-well plate) for 16 h and treated with 10 μl of AMT-101 or rhIL-10 (serially diluted in PBS) in duplicate. Following 6 h at 37°C with 5% CO_2, cells were incubated with PathHunter Flash detection reagents at room temperature (RT) for 1 h and the chemiluminescence signal read using the SpectraMax iD3 plate reader (Molecular Devices, San Jose, CA). rhIL-10 was obtained from Enzo Life Sciences.

PBMC isolation and analysis by flow cytometry

Blood samples from healthy donors were diluted 1:1 with PBS and overlaid onto 15 ml of Ficoll-Paque PLUS (GE Healthcare, Chicago, IL) in 50-ml conical tubes that were centrifuged 930 × *g* at RT for 20 min with slow acceleration and deceleration without braking. The buffy coat layer generated between the erythrocyte and serum fractions was isolated and washed twice with HBSS containing 2% FBS. Isolated cells were counted and cryopreserved in aliquots of CryoStor CS10 freezing media (STEMCELL Technologies, Cambridge, U.K.) in liquid nitrogen until use. For flow cytometry analysis, cryopreserved PBMCs were thawed and rested overnight in RPMI medium supplemented with 10% FBS, penicillin (100 U/ml), and streptomycin (100 μg/ml) at 37°C in 5% CO_2. Cells were seeded at 1×10^6/ml/well of a 24-well plate. Stocks (×100) of Chx386 or AMT-101 were added to wells in triplicate, and cells were incubated at 37°C for 20 h. Media was replaced with 1 ml of fresh complete RPMI 1640 containing 10 ng/ml LPS and brefeldin A to inhibit intracellular protein transport. Cells were then incubated at 37°C for a further 4 h. For immune sandwich analysis, rested PBMCs were seeded in a 96-well plate at 1×10^5 cells/200 μl/well. After incubating with AMT-101 or Chx386 for 20 h, cells were stimulated with 0.01 ng/ml LPS in fresh media lacking brefeldin A for 4 h. Cell culture supernatants were collected and analyzed using the human inflammatory panel V-PLEX assay (Meso Scale Discovery, Rockville, MD). The LPS concentration used to prime cells in these immune sandwich studies was identified by testing concentrations from 0.001 to 100 ng/ml for induction of TNF-α secretion by PBMCs (data not shown).

IL-10 immunoassay

This assay was used to measure what we will refer to as total IL-10 in plasma and tissue lysates. The mAb pair in this sandwich immunoassay reacts with both hIL-10 and nonhuman primate (NHP) IL-10. Therefore, total IL-10 refers to the rhIL-10 portion of AMT-101, any fragments of AMT-101 that contain intact IL-10 epitopes that are recognized by the Ab pair, and endogenous cynomolgus IL-10. Samples were quantitated using a standard curve prepared from AMT-101 calibrator and reported as picomolarity of total IL-10. For plasma, 25 μl diluent 43 was added to the Meso Scale Discovery (MSD) four-spot format IL-10 plate and incubated with shaking for 0.5 h. Controls and standards were prepared in pooled, untreated cynomolgus plasma (BioIVT). Standards, controls, and samples (25 μl each) were added to the assay plate and incubated at RT for 2 h with shaking. Plate were washed thrice with PBS with Tween 20 (PBST) before 1× SULFO-TAG anti–hIL-10 Ab that was added prior to incubation for 1 h at RT with shaking. Following a wash step, 2× MSD Read Buffer was added and the plate read in the MSD QuickPlex SQ 120 plate reader. The lower limit of quantitation for this assay was 0.2 pM total IL-10.

AMT-101 immunoassay

Detection of AMT-101 in plasma and tissue lysates follows a similar protocol as the total IL-10 immunoassay. The capture Ab in this sandwich immunoassay reacts with both hIL-10 and NHP IL-10; however, the detection Ab (1.5 μg/ml, diluted in diluent 3) binds to Chx386. This Ab pair maximizes the chances that the analyte detected in this assay is intact AMT-101. Samples were quantitated using a standard curve prepared from AMT-101 and reported as picomolarity of AMT-101. The lower limit of quantitation for this assay was 1.6 pM of AMT-101.

STAT3 phosphorylation assay

Mouse macrophage J774.41 cells (TIB67; American Type Culture Collection) were seeded at 100,000 cells per well of a 96-well plate in 100 μl of serum-supplemented cell culture media (DMEM high glucose with 10% FBS) and incubated overnight. AMT-101 and IL-10 were serially diluted in PBS, and 10 μl aliquots were added to cells in duplicate. After 20 min of incubation at 37°C, the cell culture media was removed, and cell lysates prepared and assayed for phospho-STAT3 and total STAT3 (MSD; Rockville, MD). Electrochemiluminescence signals were read on a QuickPlex SQ 120 plate reader (MSD); respective signals were presented as a ratio.

Murine proinflammatory cytokine panel

Cytokines were evaluated using a multiplex sandwich immunoassay kit (MSD) using assay plates precoated with capture Abs on independent and predefined spots; samples were quantitated against a standard curve prepared using a mixture of the cytokines from MSD. The precoated plate was washed three times with PBST before use. Standards were prepared in diluent 2, and test samples are diluted 2-fold in diluent 2. Plates were incubated with standards and diluted samples, followed by incubation with the capture Abs before signals were read per manufacturer's protocol.

NHP IL-1Ra immunoassay

Endogenous IL-1R antagonist (IL-1Ra) in NHP (cynomolgus monkey) plasma was measured using the NHP IL-1Ra U-PLEX assay (MSD). The Ab pair in this sandwich immunoassay reacts with both human and NHP IL-1Ra. Samples were quantitated using a standard curve prepared from a human IL-1Ra calibrator. Biotinylated anti-NHP IL-1Ra capture Ab was added to a Small Spot Streptavidin plate and incubated for 1 h at RT with shaking. Controls were prepared in pooled cynomolgus plasma (BioIVT), standards (calibrator 9 blend) were prepared in diluent 43, and samples were diluted 10-fold in diluent 43. Standards, controls, and diluted samples were added to the assay plate and incubated for 2 h at RT with shaking. After washing the plate three times with PBST, 1× SULFO-TAG anti–IL-1Ra Ab was added and incubated for 1 h at RT with shaking. Following a wash step, 2× MSD Read Buffer was added, and the plate was read in the MSD QuickPlex SQ 120 plate reader. The same procedure, with the following adaptation, was used to analyze tissue lysates: assay diluent for tissue analysis was T-PER buffer with 0.4% BSA, and wells were blocked with tissue lysis buffer containing 1.5% BSA prior to the addition of samples. The lower limit of quantitation for this assay was 50 pg/ml IL-1Ra.

In vitro transport

Confluent monolayers of human small intestinal tissues (SMI-100; MatTek, Ashland, MA) established on cell culture inserts were allowed to stabilize for 24 h at 37°C prior to use. Only inserts having a *trans*-epithelial electric resistance of >400 $\Omega \bullet cm^2$ were considered to have sufficient monolayer integrity for use in studies. A secondary verification of monolayer integrity was performed by assessing suppression of 70-kDa dextran transport, with detectable levels of transport after 15 min demonstrating defective barrier function. Monolayers were washed once with transport buffer (PBS) before test molecules were applied to the apical surface in 100 μl volumes. Basolateral volumes of 500 μl PBS were replaced at each time point for transport studies. Each experimental condition was performed in triplicate.

In vivo transcytosis

Male Wistar rats, housed three to five per cage with a 12/12-h light/dark cycle, were 225–275 g (~6–8 wk old) when placed on study. For dose administration by intraluminal injection (ILI), all experiments were conducted during the light phase using a nonrecovery protocol that used continuous isoflurane anesthesia. A 4–5-cm midline abdominal incision exposed mid–jejunum regions. Stock solutions of test articles were prepared in PBS so that 3.86×10^{-5} M in a 50-μl volume could be administered by ILI using a 29-gauge needle. The mesentery adjacent to the ILI site was denoted with using a permanent marker. At study termination, a 3–5-mm region that captured the marked intestine segment was isolated and processed for microscopic assessment. All experiments were performed in accordance with the U.K. Animals (Scientific Procedures) Act of 1986, the European Communities Council Directive of 1986 (86/609/EEC), and the University of Bath's ethical review procedures. In the case of oral gavage, rats received a 200-μl dosing solution of 200 mM $NaHCO_3$ (pH 8.5) containing FITC-conjugated BSA from Sigma-Aldrich (St. Louis, MO).

Immunofluorescence microscopy

Isolated intestinal tissues were fixed in 4% paraformaldehyde at 4°C for 18–24 h, processed using a Leica TP1020 tissue processor, dehydrated in increasing concentrations of ethanol, cleared with HistoClear (National Diagnostics), and infused with molten paraffin wax. Sections cut from tissue-embedded paraffin wax blocks (5-μm thickness; Jung Biocut2035 microtome) were mounted on glass microscope slides, rehydrated, and processed for Ag retrieval by boiling slides in 10 mM sodium citrate for 10 min, followed by washing with PBS. Processed tissue slices were permeabilized using 0.1% Triton X-100 in PBS for 30 min, blocked using 2% donkey or goat serum and 2% BSA in 0.1% Triton X-100 in PBS for 2 h, and incubated overnight at 4°C with primary Abs diluted in 1% BSA and 0.05% Triton X-100 in PBS at 4°C. Tissue slices were washed thrice with PBS, incubated for 2 h with secondary Abs conjugated to Alexa Fluor fluorescent dyes, washed thrice with PBS, and incubated for 1 h with 200 nM DAPI, washed with PBS, dehydrated in ethanol, and covered by mounting a coverslip with Fluoroshield (Abcam) mounting media; all steps were performed at RT unless otherwise noted.

Primary Abs. Primary Abs included the following: rabbit anti–hIL-10 (ab34843; Abcam), goat anti–hIL-10 (ab10775; Abcam), rabbit pSTAT3 (ab76315; Abcam), rat anti-mCD3 (ab11089; Abcam), rat anti-mF4/80 (ab6640; Abcam), internally generated rabbit and mouse anti-Chx Abs; mouse anti-EEA1 mAb (ab70521; Abcam), mouse anti-LAMP1 mAb (ab25630; Abcam), mouse anti-Rab7 mAb (sc-376362; Santa Cruz Biotechnology), mouse anti-Rab11a mAb (sc-166912; Santa Cruz Biotechnology), mouse anti-TGN38 mAb (NB300-575; Novus), mouse anti-clathrin mAb (ab2731; Abcam), and mouse anti-calnexin mAb (sc-23954; Santa Cruz Biotechnology).

Secondary Abs. Secondary Abs included the following: donkey anti-mouse IgG Alexa Fluor 647 (A31571; Invitrogen), donkey anti-rabbit IgG Alexa Fluor 546 (A10040; Invitrogen), donkey anti-goat IgG Alexa Fluor 488 (A11055; Invitrogen), donkey anti-goat IgG Alex Fluor 488 (A-11055; Abcam), donkey anti-rabbit IgG Alex Fluor 647 (A-31573; Abcam), and donkey anti-rat IgG Alexa Fluor 555 (A150154; Abcam).

After allowing the mounting media to dry at 4°C overnight, fluorescent images were obtained using a Zeiss 880 LSM confocal microscope, a PerkinElmer Vectra, or a Leica SP5 inverted confocal microscope using the following settings: excitation/emission wavelengths used for the various fluorophores were the following: DAPI (405 nm/462 nm), Alexa Fluor 488 (488 nm/562 nm), Alexa Fluor 564 (561 nm/602 nm), and Alexa Fluor 633 (633 nm/693 nm). For confocal microscopy, the pinhole was set between 0.99 and 1.22 airy units to achieve a z-resolution of 0.8 μm. All laser intensities were set at 2%. All images were captured with a total magnification of ×10–×630. Image analytics software included Zeiss Zen 2.6 Blue software, Leica SP5, PerkinElmer Phenochart, Inform, Imaris, and ImageJ.

IL-1Ra

Mice. Female SJL/J mice (7–8 wk of age) were administered a 10 mg/ml solution of AMT-101 by oral gavage. Blood and intestinal tissue samples were collected at 0 (predose), 1, 2.5, and 4 h postdose for ELISA-based measurement of hIL-10 and IL-1Ra.

NHP. Male cynomolgus monkeys (n = 3 per group) received pancolonic administration of 1, 3, or 10 mg AMT-101 (total dose) via the rectal route using a colonoscope connected to a spray nozzle with a 360° spray pattern. Serial tissue biopsy samples were collected by sigmoidoscopy at predose and 0.25, 0.5, 0.75, 8, and 24–28 h postdose. Serial plasma samples were collected at predose and at set times through 24–28 h postdose.

Studies involving murine models of induced intestinal inflammation

T cell transfer. On study day 0, nine SCID mice received a 200-μl i.p. injection containing 4×10^5 $CD4^+$ $CD45RB^{high}$ T lymphocytes isolated from the spleens of 28 BALB/c mice (12 wk old). On study day 34, nine BALB/c mice and 12 SCID mice, including nine with the colitis-like model of inflammation, were dosed with ~160 pM of AMT-101 or rhIL-10, or PBS, via a 20-μl ILI into the distal ileum as well as the proximal, middle, and distal colon. In each group, two mice were terminated at 10 min, and one was terminated at 40 post-ILI when intestinal tissues and plasma or serum was collected. Collected tissue was fixed, embedded, sectioned, and stained with H&E for histological assessment to confirm inflammatory status. ELISA analysis to measure hIL-10 was performed on lysates prepared from intestinal tissue and plasma or serum.

Dextran sulfate sodium. Eight- to ten-week-old female C57BL/6 mice were given 2.5% dextran sulfate sodium (DSS) in their drinking water (ad libitum) for 7 d to induce colitis and dosed orally once daily for 10 d with vehicle (10 mg/ml soybean trypsin inhibitor in 0.2 M $NaHCO_3$), 75 mg/kg cyclosporine A, 9 mg/kg rhIL-10, or 0.3, 3, 10, or 30 mg/kg AMT-101 (Supplemental Fig. 5). Body weight was recorded daily from day −5 to

day 7. Disease activity index was also evaluated and included daily measurement of body weight, evaluation of stool consistency, and presence of hemoccult. Tissue and plasma or serum samples were collected 4 h after final dose for histopathology as well as to determine colon length and weight.

Oxazolone. Seven- to eight-week-old female SJL/J mice were presensitized with oxazolone (Oxa) on day −5 and, 5 d later on day 0, were challenged intrarectally with Oxa (Supplemental Fig. 5). Control mice (naive; $n = 5$) were dosed with vehicle and presensitized and rectally challenged with ethanol rather than Oxa. Remaining groups were dosed with vehicle ($n = 10$), AMT-101 (8.45 mg/kg; $n = 15$), or 5-aminosalicylic acid (5-ASA; 100 mg/kg; $n = 15$) after presensitization and subsequent intrarectal challenge with Oxa from day −5 to day 6 for a total of 12 doses. Body weight was recorded daily from day −5 to day 7. Fecal consistency and occult blood positivity were recorded after intrarectal administration of Oxa from day 1 to day 7. Disease activity index (body weight, evaluation of stool consistency, and presence of hemoccult) was determined daily. Animals were sacrificed on day 7 and blood samples collected. Distal colon sections were subjected to histopathological analyses by H&E staining that was scored for disease severity by a board-certified veterinarian pathologist using the following scoring scheme: 0, no sign of inflammation; 1, very low level of inflammation; 2, low level of leukocytic infiltration, low level of inflammation; 3, high level of leukocytic infiltration, high vascular density, inflammation, and thickening of colon wall; and 4, transmural infiltration, loss of goblet cells, high vascular density, crypt abscesses, thickening of colon wall, and ulceration.

Statistics

Statistical analyses were performed using Prism 7.0 (GraphPad Software). Any p values ≤0.05 were considered significant.

Results

AMT-101 is a dimer capable of activating the hIL-10R in vitro

Classified as a class 2–type cytokine, hIL-10 is a homodimer with subunits of 178 aa; interactions between two IL-10 homodimers and four IL-10R components appear critical for its signaling (22, 24). To create the hIL-10 payload vector, the Chx386 was genetically conjoined at its C terminus through a series of glycine and serine (GS) residues to the N terminus of the hIL-10 monomer (Fig. 1A). Chx386 is a nontoxic fragment of the full-length Chx protein designed by truncating the C-terminal domain III of the exotoxin that enzymatically ADP ribosylates elongation factors in nonpolarized cells to block protein synthesis and incite apoptosis (17). Published structural data for Chx (Protein Data Bank identification number: 2Q5T) and hIL-10 (Protein Data Bank identifier: 1J7V) were used in designing the GS amino acid connector sequence to allow for uninhibited dimerization of the hIL-10 monomer elements during refolding and for hIL-10 dimer access to its cognate receptor when conjoined to Chx386. AMT-101, expressed in *E. coli*, refolded from inclusion bodies, and purified (>95%), was verified for accurate fusion protein m.w. via SDS-PAGE, and the anticipated monomer molecular mass of ∼62,900 Da for AMT-101 monomer was observed (Fig. 1B). Absolute masses of the folded dimer (125,796.41 Da) and unfolded monomer (62,898.21 Da) were verified by mass spectroscopy (Supplemental Fig. 1). A best-fit small-angle x-ray scattering analysis of the protein fragments in solution was consistent with the designed AMT-101 structure (Fig. 1C).

AMT-101 is biologically active in vitro

Functional assessment of Chx386 to transport hIL-10 across the intestinal epithelium was verified using polarized, confluent monolayers of human small intestinal cells cultured on semipermeable membranes in vitro (Fig. 2A). Despite the much larger molecular mass, AMT-101 transported across these monolayers to a greater extent than rhIL-10, demonstrating that the Chx386 domain of AMT-101 retains its capacity to undergo apical to basal (A→B) transcytosis. AMT-101 was next tested in vitro to ensure that the hIL-10 element of the fusion protein was biologically

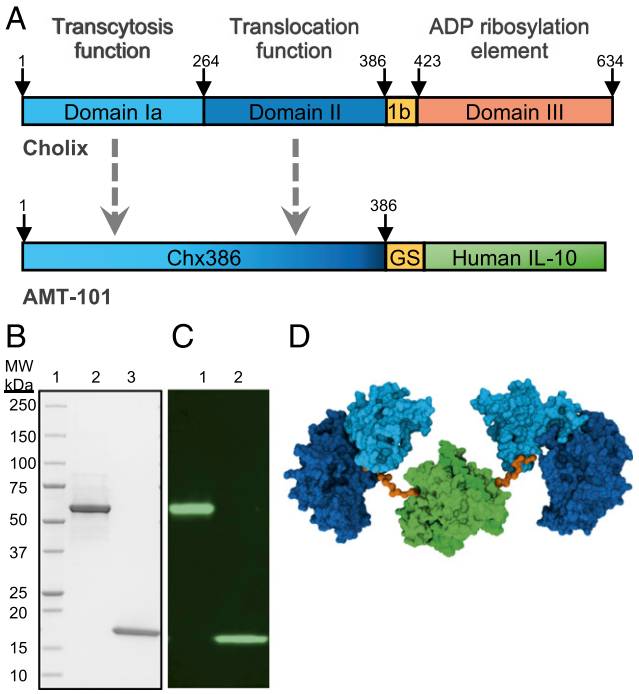

FIGURE 1. AMT-101 is a recombinant fusion protein of Chx and IL-10. (**A**) Full-length Chx was truncated to Chx386, comprised of domains IA and II, and genetically conjoined to hIL-10 via a glycine–serine linker (GS). (**B**) SDS-PAGE of m.w. standards (lane 1), AMT-101 (lane 2), and commercial rhIL-10 (lane 3) showing monomeric AMT-101 and IL-10. (**C**) A fluorescent murine anti–hIL-10 Western blot of the previous SDS-PAGE showing AMT-101 (lane 1) and rhIL-10 (lane 2). (**D**) Solution structure of AMT-101 adapted from small angle x-ray diffraction data of the Chx and hIL-10 elements. Chx386 element (blue), GS linker (orange), and hIL-10 dimer (green) are depicted.

active. The U2OS osteosarcoma cell line engineered to express the two receptors involved in IL-10 signal transduction (IL-10R1 and IL-10R2) that exhibit a luminescence event as a result of ligand-induced receptor dimerization was used to test increasing doses of AMT-101, rhIL-10, or Chx386. AMT-101 had an EC_{50} of 971.4 pM compared with 91.53 pM for rhIL-10 (Fig. 2B), whereas Chx386 alone did not induce IL-10R dimerization. To assess downstream potency, the potential for AMT-101, rhIL-10, or Chx386 to induce phosphorylation of STAT3 was examined using mouse macrophage J774.2 cells. AMT-101 demonstrated an EC_{50} of 263.6 pM compared with 40.98 pM for a commercial preparation of hIL-10 in this assay (Fig. 2C). Notably, AMT-101 had a reduced amplitude of pSTAT3/total STAT3 of ∼1.47% compared with hIL-10 at 2.19%. Finally, pretreatment of human PBMCs with AMT-101 resulted in a dose-dependent reduction of secreted TNF-α and surface expression of HLA-DR, but not secreted IL-6, normally induced by endotoxin (LPS) treatment in this treatment scenario (Fig. 2D–F). Chx386, alone, did not affect TNF-α or HLA-DR levels. In the presence or absence of endotoxin, neither AMT-101 nor Chx386 treatment of PBMCs induced the secretion of inflammatory markers such as IFN-γ, IL-1β, IL-2, IL-4, or IL-6 (data not shown). Together, these data show that conjoining hIL-10 to Chx386 through a GS polypeptide sequence spacer produced a chimera that retained the desired properties required for AMT-101 to reach cells within the intestinal lamina propria and to activate IL-10R signaling pathways in that compartment. The reduction in IL-10R dimerization and extent of pSTAT3 induction observed for AMT-101 compared with hIL-10 were likely due to steric hinderance and/or possible Chx386 interactions with other cell-surface

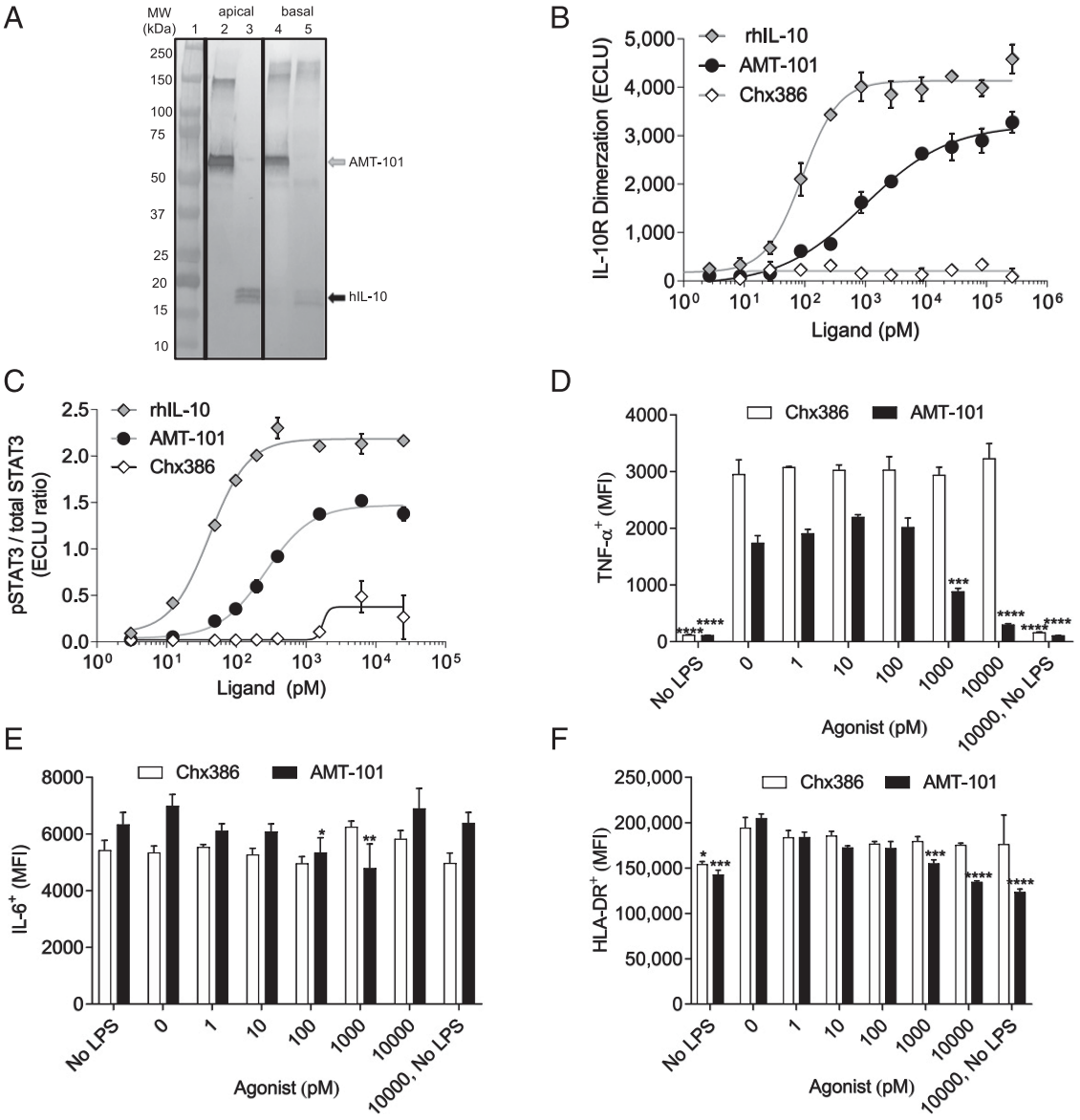

FIGURE 2. The elements of AMT-101 are functionally active in vitro. (**A**) In an intestinal model system of confluent, polarized human SMI-100 monolayers, an anti–hIL-10 Western blot detects the extent of equimolar applications of AMT-101 (lane 2, apical, $t = 0$ h), or commercial hIL-10 (lane 3, apical, $t = 0$ h) transiting to the basal compartment of respective Transwells (lane 4, AMT-101, basal, $t = 2$ h; and lane 5, hIL-10, basal, $t = 2$ h). Lanes from a single Western blot were spliced together to facilitate comparisons and are indicated by black lines. (**B**) Dimerization of IL-10A and IL-10B receptors engineered into U2OS osteosarcoma cells induced by ATM-101 or hIL-10 after 6 h. (**C**) Induction of STAT3 phosphorylation, relative to total STAT3 content, in a mouse macrophage-like cell line J774.2 after 20 min of stimulation. Data are representative of multiple studies with similar results. (**D**–**F**) Flow cytometry analysis of gated, live $CD45^+$ $CD14^+$ monocytes (PBMCs) obtained from healthy, human donors showing IL-10's suppressive effect on LPS-induced (D) TNF-α secretion, (E) IL-6 secretion, or (F) surface expression of HLA-DR; data of mean fluorescence intensity (MFI) as means ± SEM ($n = 3$) analyzed by two-way ANOVA with Dunnett post hoc test. $*p < 0.5$, $**p < 0.01$, $***p < 0.001$, $****p < 0.0001$, when compared with 0 pM concentration values.

elements on these cells. Such in vitro differences were assumed to become less relevant in vivo because of the capability of AMT-101, but not hIL-10, to undergo epithelial cell transcytosis and efficiently reach the intestinal lamina propria.

Transcytosis of AMT-101 in vivo

As a biopharmaceutical, clinical use of AMT-101 will require administration using an enteric-coated oral dosage form to protect it during gastric transit and for its deposition in the late ileum to proximal colon segments of the gastrointestinal tract as a way to target sites of intestinal inflammation. To test AMT-101 for its effects by repeat dosing in rodents that cannot be readily pilled, we explored the use of oral gavage administration by assessing the distribution of FITC-labeled BSA (Supplemental Fig. 2). These studies demonstrated that a protein delivered by oral gavage would reach the jejunum and ileum after 60 min, be predominantly in the ileum by 90 min, and could reach the colon by 180 min. It is important to note that in this oral gavage model, it is unclear 1) how much of the administered dose leaves the stomach and 2) the fraction of that dose that reaches the distal ileum and colon that is still biological active.

With these oral gavage dosing concerns in mind, we next asked the question of whether AMT-101 can undergo efficient transcytosis in vivo by examining pSTAT3 induction in rat intestinal tissue isolated 40 min after oral gavage with PBS, rhIL-10, or AMT-101. Immunofluorescence microscopy of tissues from PBS-treated animals failed

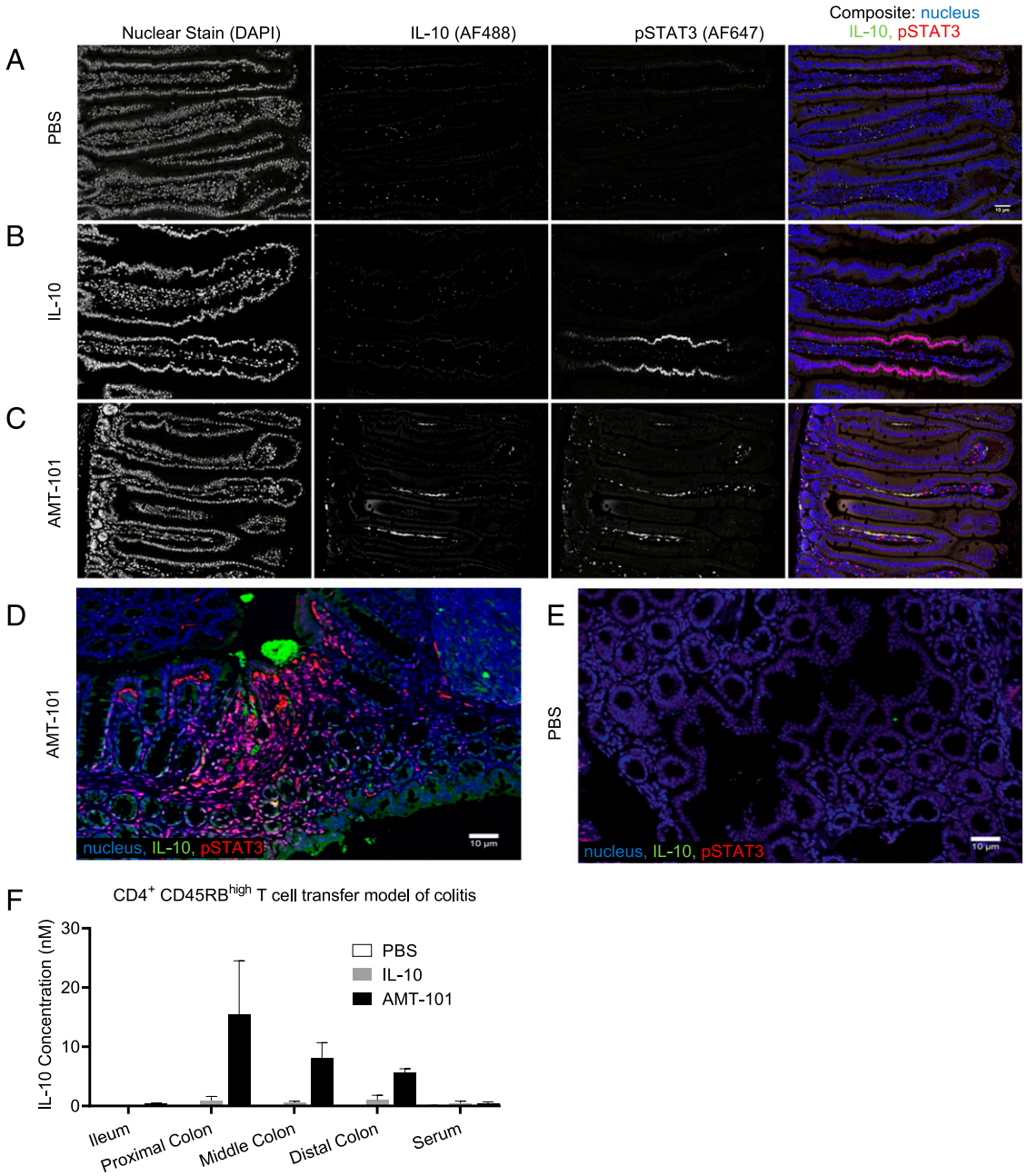

FIGURE 3. Transcytosis of AMT-101 and induction of phosphorylated STAT3 in vivo. BALB/c$^{il10-/il10-}$ mice were orally gavaged with (**A**) PBS, (**B**) hIL-10, or (**C**) AMT-101. Single-channel images were captured and merged into a composite with nuclei (blue), IL-10 (green), and pSTAT3 (red). (**D**) AMT-101 and (**E**) 1× PBS in WT BALB/C colon after ILI were imaged with the same color scheme as above. (**F**) In the inflamed T cell transfer model, an hIL-10 ELISA was run with PBS, IL-10, and AMT-101 after ILI on the indicated intestinal tissues and plasma; representative images are shown for $n = 3$ per treatment in (A)–(E), and $n = 2$ for (F). Scale bar, 10 μm for respective datasets.

to exhibit any immuno-reactivity for hIL-10 or pSTAT3 induction in either the lamina propria or intestinal epithelium (Fig. 3A). In some instances, rhIL-10–dosed animals exhibited pSTAT3 induction in enterocytes, but not in cells within the lamina propria; no hIL-10 within the tissue was detected (Fig. 3B). This observation is consistent with findings in mice that intestinal epithelial cells can express IL-10Rs at their apical surface under certain conditions associated with development and maintenance of barrier function (25). Tissues isolated from animals treated with AMT-101 demonstrated extensive amounts of hIL-10 and a large number of cells that were positive for pSTAT3 within the lamina propria (Fig. 3C).

We next examined the transport of AMT-101 across inflamed intestinal tissue. A mouse model of colitis induced by transfer of CD4$^+$ CD45RB^{high} T cells (26) was used in an ILI format to focus the dose and targeting of ~160 pM of AMT-101 or rhIL-10 into the distal ileum or proximal, mid, or distal regions of the colon in PBS (Fig. 3F). Histopathological microscopic assessment of intestinal tissues confirmed inflammation at all levels of the colon, but not in the ileum. At 10 min post-ILI, distal ileum tissues contained ~5-fold higher levels of hIL-10 for AMT-101 compared with rhIL-10 treatment; in inflamed tissue, hIL-10 levels measured after ILI of AMT-101 were ~10-fold higher compared with rhIL-10 treatment (Fig. 3F). The higher tissue levels of hIL-10 observed in inflamed colon relative to noninflamed distal ileum was likely due to differences in barrier properties of these tissues. Tissues examined at 40 min post-ILI suggested that hIL-10 delivered via

AMT-101 mirrored the data obtained at 10 min with a greater relative uptake being observed in the noninflamed distal ileum (data not shown). Importantly, AMT-101 was not observed in the systemic circulation (Fig. 3F).

Proximal colon tissues collected from an ILI site in BALB/c mice treated with AMT-101 or rhIL-10 were also evaluated for pSTAT3 and hIL-10 by immunofluorescence microscopy. In one sample, some nonabsorbed AMT-101 was observed in the lumen as a precipitate resulting from the dehydration steps during sample preparation; adjacent to this precipitate was extensive induction of cellular pSTAT3 (Fig. 3D). Activation of pSTAT3 in the cytoplasm was observed as the red fluorescent channel with subsequent nuclear translocation of pSTAT3 being observed as magenta because of colocalization with the blue (DAPI) nuclear stain. A comparable site where PBS was administered by ILI failed to show a similar level of pSTAT3 induction (Fig. 3E).

We next wanted to ensure that the genetic construction of AMT-101 retained the A→B transcytosis properties that should be imparted by Chx, which was previously shown to undergo receptor-mediated uptake and vesicular trafficking without targeting to the lysosomal degradation pathway in polarized enterocytes (19). Chx386 and hIL-10 elements of the fusion protein AMT-101 remained together during A→B transcytosis and within the lamina propria, allowing localization of hIL-10 to accurately describe the distribution of AMT-101 (Supplemental Fig. 3A). Although Rab7$^+$ vesicles (defining late endosomes) were present in both apical and basal vesicular compartments of enterocytes, colocalization with AMT-101 occurred predominantly in the apical vesicular compartment (Supplemental Fig. 3B). Rab11$^+$ vesicles (defining recycling endosomes) were also observed in both the apical and basal compartments of enterocytes but, opposite to Rab7, colocalizations with AMT-101 occurred mostly in the basal vesicular compartment (Supplemental Fig. 3C). AMT-101 colocalized with Rab11 to a greater extent compared with Rab7 within cells in the lamina propria (Supplemental Fig. 3B, 3C), consistent with distinct Chx-mediated trafficking events in polarized versus nonpolarized cells.

Lectin, mannose binding 1 (LMAN1) protein, a resident of the endoplasmic reticulum–Golgi intermediate compartment and known to be involved in the sorting or recycling of proteins and lipids, is involved in Chx transcytosis (19). AMT-101 also colocalized with LMAN1 that redistributes within enterocytes during A→B transcytosis (Supplemental Fig. 3D): at 1 min, when AMT-101 was just entering at the luminal membrane, LMAN1 was localized in the apical compartment; at 5 min, LMAN1 and some of the internalized AMT-101 were present in the supranuclear region associated with endoplasmic reticulum–Golgi intermediate compartment distribution; by 10 min, AMT-101 and LMAN1 were extensively colocalized in the basal compartment; and by 15 min, the extent of LMAN1 redistribution and colocalization with AMT-101 throughout the enterocyte was maximized. The timing of LMAN1 redistribution to the basal compartment coincides with the presence of hIL-10 being detected in nonpolarized cells within the lamina propria, where it was not associated with LMAN1. This redistribution of LMAN1 associated with AMT-101 A→B transcytosis is identical to that previously observed for Chx (19).

The A→B transcytosis pathway accessed by Chx has been shown to intersect with Rab7$^+$ and LAMP1$^+$ vesicles; although these are markers of both late endosomes and lysosomes, Chx does not appear to traffic to lysosome-like structures within enterocytes (19). To examine this point for AMT-101, a time course of LAMP1 and AMT-101 colocalization was performed (Supplemental Fig. 3E). Limited LAMP1/AMT-101 colocalizations were observed in polarized enterocytes at 1 min post-ILI, with the extent of these not increasing over the 15 min time course required for completion of AMT-101 A→B transcytosis. LAMP1$^+$ structures in nonpolarized cells within the lamina propria did not show colocalization with AMT-101 at 1 and 5 min post-ILI. There were, however, extensive LAMP1/AMT-101 colocalizations in nonpolarized cells within the lamina propria at 10 and 15 min post-ILI, consistent with distinct Chx-mediated trafficking events in polarized versus nonpolarized cells. Together, these data suggest that AMT-101 A→B transcytosis was completed over a time course of 10–15 min and involved apical compartment Rab7$^+$ vesicles, basal compartment Rab11$^+$ vesicles, LMAN1 redistribution, and avoidance of lysosomal fate in enterocytes similar to that observed previously for Chx A→B transcytosis (19). Ultimately, AMT-101 is delivered to lysosome-like structures within a large fraction of cells within the lamina propria, an outcome that would limit its systemic distribution following A→B transcytosis.

Macrophages in the lamina propria are activated by AMT-101

After determining AMT-101 was biologically active in vivo, its cellular targeting within the lamina propria was investigated in mouse jejunum tissue (Fig. 4). At 40 min after oral gavage, hIL-10 was observed in the basal region of enterocytes and in linear organizations within the lamina propria that were consistent with lacteals and/or vascular vessels. Areas adjacent to detected hIL-10 demonstrated strong pSTAT3 expression in many cells within the lamina propria and, to much lower levels, in some nuclei of polarized enterocytes. A moderate proportion of CD3$^+$ cells within the lamina propria were observed to colocalize with pSTAT3; that is, many CD3$^+$ cells present within this compartment were not pSTAT3$^+$, and many pSTAT3$^+$ cells were not CD3$^+$ (Fig. 4C). Using the macrophage-specific marker F4/80, however, we observed an extensive colocalization with pSTAT3 (Fig. 4D, 4E). Additional examples of F4/80 and pSTAT3 labeling are highlighted in tissue samples obtained from the small intestine (Fig. 4F, 4G) or colon (Fig. 4I) following gavage dosing of AMT-101 in mice. These results were consistent with extensive IL-10 activation of macrophage cell populations within the lamina propria. Clearance of AMT-101 in the lamina propria appeared to occur through the Chx386 component being sequestered by CD3$^+$ cells, but not those expressing the B cell marker CD19, the endothelial cell marker CD34, or the Ag presentation marker CD11c (Supplemental Fig. 4). Together, these results suggest that AMT-101 ultimately targeted CD3$^+$ T lymphocytes following A→B transcytosis, apparently through interactions driven by its Chx386 element, whereas macrophage were extensively targeted by the hIL-10 element.

Circulating IL-1Ra and systemic hIL-10 increases in response to AMT-101 oral gavage in mice

The inflammatory actions of IL-1β are modulated by the presence of a specific receptor antagonist known as IL-1Ra (27). Increased plasma IL-1Ra levels can be induced by IL-10, which can occur in the absence of a proinflammatory state (28). With an appreciation of uncertainties associated with how much and when biologically active AMT-101 is released from the stomach to reach the small intestine as well as the timing of its uptake and actions within the lamina propria following oral gavage, we examined IL-1Ra as a biomarker of AMT-101 actions in noninflamed mice. Oral gavage of 10 mg/kg AMT-101 resulted in ∼50 pM hIL-10 being detected in systemic circulation as early as 1 h, which increased to ∼700 pM at 4 h (Fig. 5A). Detection of hIL-10 in distal small intestinal (Fig. 5B) and colonic (Fig. 5C) tissues were not significantly elevated above baseline at 1 and 2.5 h but showed slight increases with high variability at 4 h; hIL-10 in small intestinal lysates were ∼10-fold higher than colonic lysates. These outcomes were consistent with the

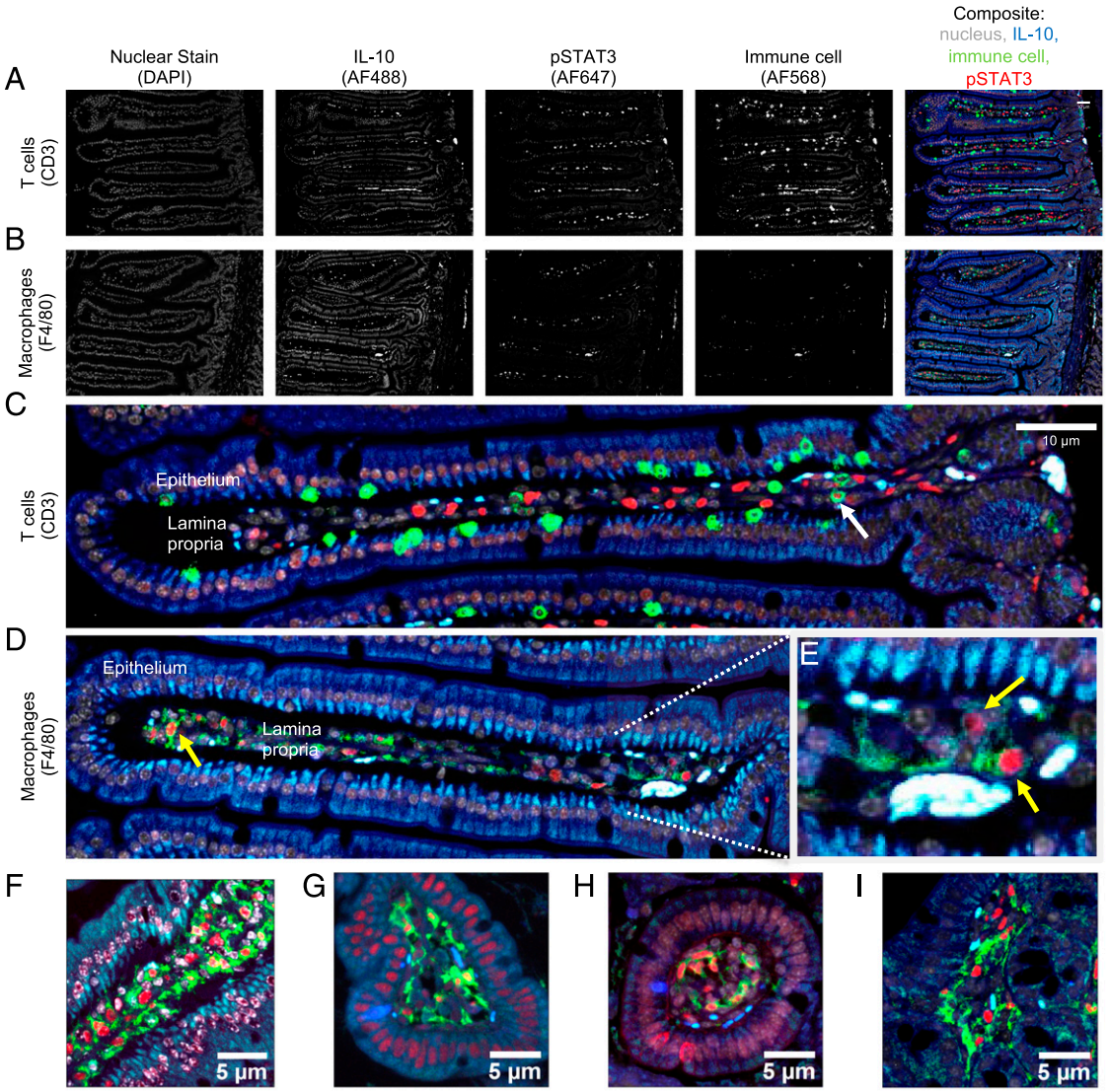

FIGURE 4. AMT-101 induces select immune cell phosphorylation in the intestinal lamina propria. To determine the identity of lamina propria pSTAT3$^+$ cells following oral gavage of AMT-101 from intestinal tissue in BALB/c$^{il10-/il10-}$ mice, immune cell populations were labeled with fluorescent Abs to either (**A**) CD3$^+$ T cell lymphocytes or (**B**) F4/80$^+$ macrophages. (**C**) A closer assessment of the CD3 stained cells showed a pSTAT3$^+$ CD3$^+$ cell with a white arrow. (**D**) A higher magnification of the F4/80-stained images reveals pSTAT3$^+$ F4/80$^+$ cells, indicated with yellow arrows. Nuclear stain (gray), IL-10 (blue), immune cells (green), and pSTAT3 (red) are shown as a composite image on the far right, whereas single-channel images are shown in the middle. (**E**) Example of an F4/80$^+$ pSTAT3$^+$ cell in the lamina propria of (D). (**F**–**H**) Additional F4/80$^+$ pSTAT3$^+$ intestinal segment examples are shown, including colon (**I**) not as a matched set. $n = 3$ per treatment. Scale bar, 10 μm for (A) and (B) set, 10 μm for (C) and (D) set, and 5 μm for (F)–(I).

retention of AMT-101 in the intestinal lamina propria that would limit its systemic distribution. These findings also support the possibility that some AMT-101 uptake occurred in the stomach and/or in the proximal small intestine to produce early levels of AMT-101 that increased marginally and inconsistently over time.

Despite the unpredictable dosing level and location within the gastrointestinal tract following oral gavage, plasma IL-1Ra levels were significantly increased at 4 h (Fig. 5D). These results demonstrated that the onset of IL-1Ra induction occurs between 2.5 and 4 h after oral gavage, about the same time as a detectable increase in tissue levels of hIL-10 was observed in distal small intestinal and colonic tissues. This result suggests that either there was a nearly immediate induction of IL-1Ra following the uptake of AMT-101 in distal small intestinal and colonic tissues or that this induction occurred several hours following the nearly rapid uptake of AMT-101 in the stomach/proximal small intestine after oral gavage. To test these possibilities, we directly deposited AMT-101 onto the luminal surface of colonic intestinal mucosa in an NHP model.

Induction of IL-1Ra following AMT-101 intracolonic spray in NHPs

A topical spraying approach was used to administer 1, 3, or 10 mg (total dose) AMT-101 onto the luminal surface of colonic mucosae (proximal, mid, and distal) of healthy, fasted NHPs (cynomolgus monkeys). This was achieved using a colonoscope with a spray nozzle attachment (29). In this way, we could obtain refined information for onset and duration of IL-1Ra induction at specific local doses. AMT-101 was detected in colonic tissues, mostly at the earliest time of 15 min that was feasible for this procedure, in a manner that was not dose dependent (Fig. 6A). Because IL-10 can induce cells to produce more IL-10 (30, 31), we also looked for induced NHP IL-10. Within 15 min after an intracolonic spray with AMT-101, dose-dependent and transient increases in tissue

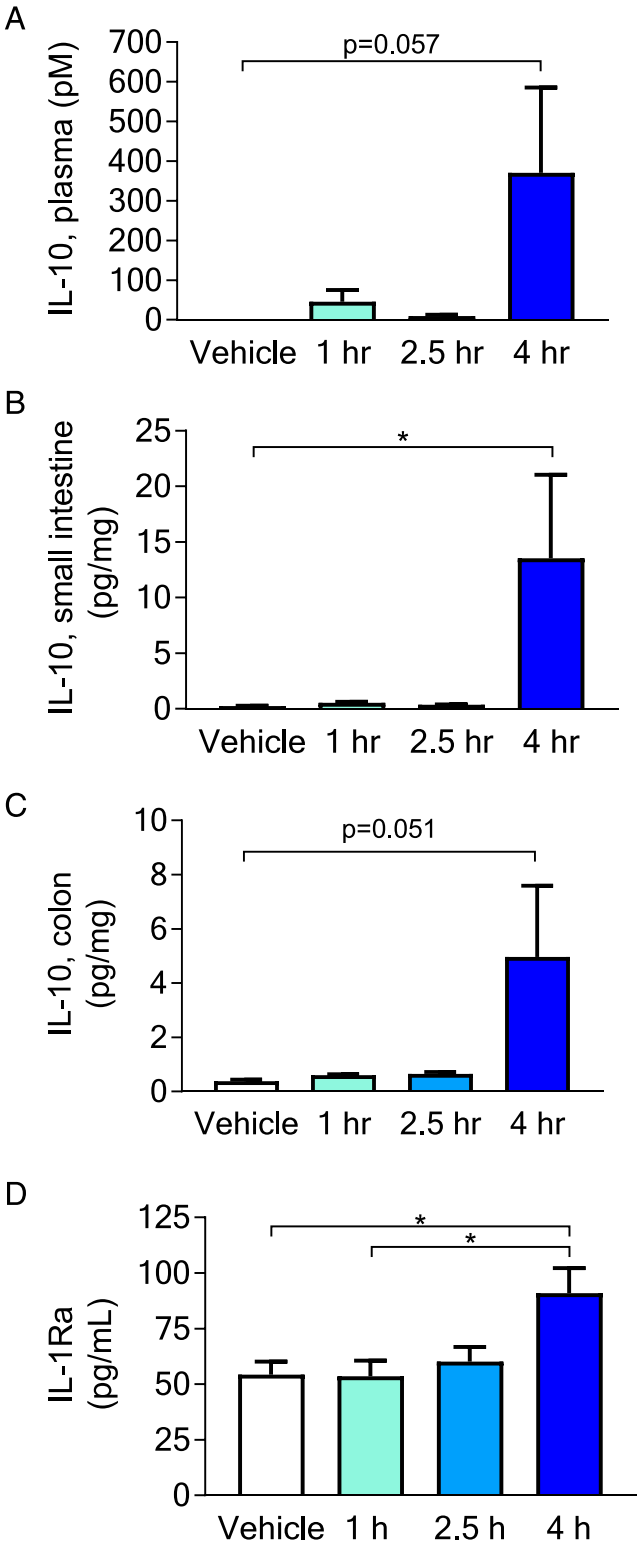

FIGURE 5. AMT-101 exposure and induction of plasma IL-1Ra in mice. Concentrations of hIL-10 in mouse (**A**) plasma, (**B**) distal small intestinal tissue, or (**C**) colonic intestinal tissue over a time course following oral gavage of 10 mg/kg AMT-101. (**D**) Plasma levels of mouse IL-1Ra over this same time course following oral gavage of 10 mg/kg AMT-101. Differences assessed by one-way ANOVA with Dunnett analysis with $n = 9$ for (A)–(C) or by one-way ANOVA with Tukey multiple comparisons test with $n = 7$–9 for (D), with mean ± SEM. *$p < 0.05$.

IL-10 levels were observed in a dose-dependent manner (Fig. 6B). Consistent with the rapid uptake and actions of AMT-101 from the intestinal luminal surface and its retention within the lamina propria, plasma levels of AMT-101 were below the assay detection limit (Fig. 6C). The amount of plasma IL-10, presumably coming from induction of monkey IL-10 by the actions of AMT-101 within the lamina propria, increased in a dose-dependent manner (Fig. 6D). Circulating levels of IL-1Ra increased strikingly between 2 and 3 h after colonic spray of AMT-101 in a manner that suggested a near saturation of this response at the lowest dose tested (Fig. 6E). These results suggested that AMT-101 delivered to the apical surface of colonocytes can initiate systemic pharmacodynamics relevant for IL-10 in the absence of a systemic pharmacokinetic profile for this cytokine. Finally, we examined pSTAT3 induction in colon tissues biopsies following topical AMT-101 application (Fig. 6F). Although it was clear that some pSTAT3 induction had occurred, this downstream element of IL-10R signaling was observed inconsistently in tissues isolated over the time course of the study. The variability of pSTAT3/total STAT3 detection was likely due to tissue capture and stability challenges in this in vivo model. Measurement of tissue AMT-101 levels had similar tissue capture and stability challenges, showing low and variable amounts in the tissue samples collected (Fig. 6A). It is important to note, because of the similarity of human and NHP IL-10, that ELISA values shown could also include hIL-10 that has somehow separated from the carrier domain of the AMT-101 molecule. Although we cannot rule this out, we have no other data to support this as an outcome and assume that the majority, if not all, tissue and plasma IL-10 measured represents an NHP source.

AMT-101 suppression of colitis-like symptoms in mice induced by DSS

We next wanted to examine the ability of AMT-101 to suppress the mild to moderate multifocal colitis induced by DSS, characterized by inflammation, edema, and mucosal necrosis when this medium-chain-length fatty acid binding agent is presented in drinking water [reviewed in (32)]. Mice were dosed orally once daily for 10 d with vehicle (as a negative control) or AMT-101 (0.3–30 mg/kg) from the induction of DSS-induced colitis (Supplemental Fig. 5). Mice dosed daily with 75 mg/kg cyclosporine A were used as a positive control for the model and not a therapeutic comparator. AMT-101 significantly reduced DSS-induced weight loss during the in-life portion of the study (Fig. 7A). Comparisons of initial and final weights showed that AMT-101 was effective in a dose-dependent manner (Fig. 7B). AMT-101 treatment, however, did not statically improve colon weight/length ratio in this model (Fig. 7C). Interestingly, a dose-dependent benefit of AMT-101 for colon length outcomes was observed (Fig. 7D), but not for colon weight (Fig. 7E). Midcolon tissue examination at study termination demonstrated improvements in inflammation-based parameters (erosion, edema, mucosal thickness, gland loss, hyperplasia, and mucosal thickness) comparable to negative controls (Fig. 7F–H). It should be noted that the oral gavage of a molar equivalent amount of rhIL-10 (9 mg/kg) as compared with AMT-101 (30 mg/kg) failed to show any therapeutic benefits in these studies (data not shown). Also, plasma samples collected at various times during these studies failed to show high plasma levels of hIL-10 that could have come from circulating AMT-101 (data not shown).

AMT-101 blocks Oxa-induced colitis in mice and correlates with inflammatory markers

The hapten Oxa-based model of intestinal inflammation, in which active colitis is established by day −5 [reviewed in Ref. 33], was used to examine the potential of AMT-101 to suppress colitis-like

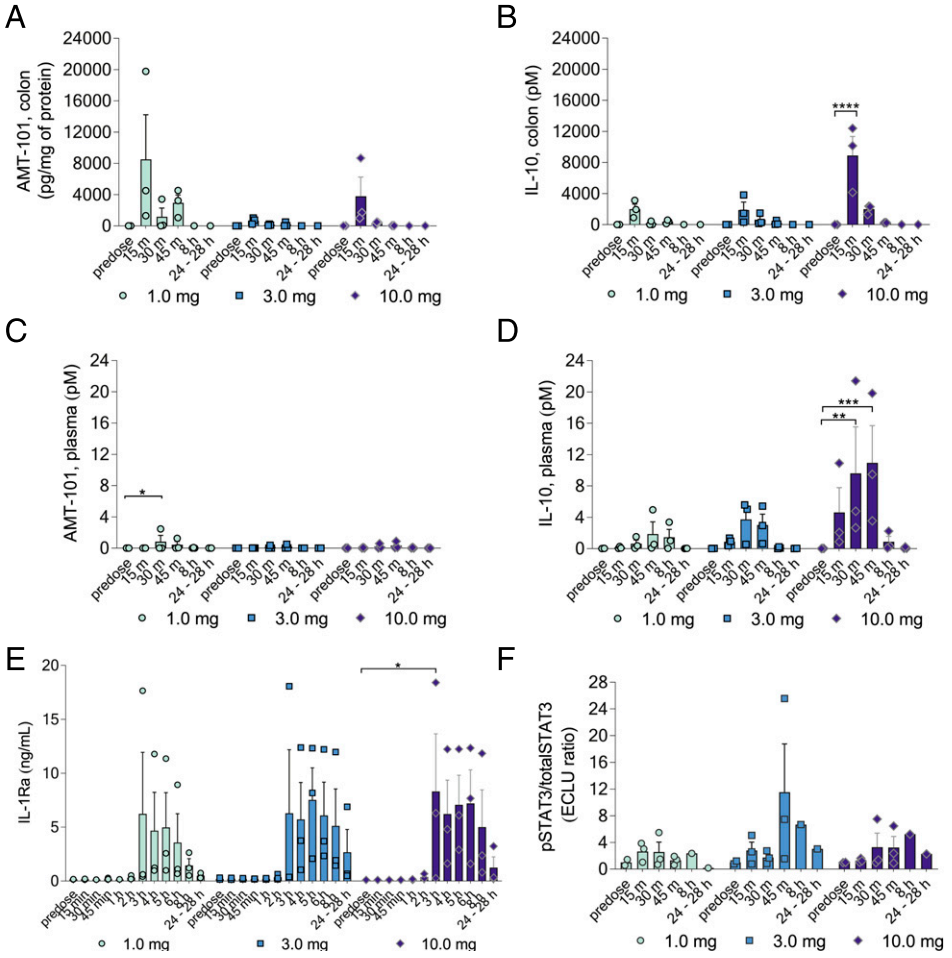

FIGURE 6. AMT-101 intracolonic spray results in local and systemic biodistribution of IL-10 and induction of plasma IL-1R in NHPs. NHPs were dosed at 1, 3, and 10 mg, and biological samples were collected at the indicated time points. Snip biopsies of colonic tissues were assessed for (**A**) AMT-101 and (**B**) hIL-10 via ELISA. NHP plasma was similarly assessed for (**C**) AMT-101 and (**D**) hIL-10. (**E**) IL-1Ra concentrations were measured in NHP plasma. (**F**) The ratio of pSTAT3 relative to total STAT3 was measured in NHP colon. Differences assessed by two-way ANOVA with Dunnett analysis. $n = 3$ per treatment for systemic measurements (C–E) and $n = 1$–3 for the NHP homogenized tissue samples (A, B, and F). Mean ± SEM. $*p < 0.05$, $**p < 0.01$, $***p < 0.001$, $****p < 0.0001$.

pathologic indices. In a prophylactic setting, 8.45 mg/kg (67 nM/kg) AMT-101 was administered daily by oral gavage every day or every other day for 12 d after presensitization and subsequent intrarectal challenge with Oxa (Supplemental Fig. 5). Control (naive) mice, presensitized, followed by intrarectal administration of ethanol (no Oxa), were used as a negative control. Oral dosing with 100 mg/kg (0.65 mM/kg) 5-ASA was used as an internal positive control to ensure model responsiveness for animals with Oxa-induced colitis but was not intended as a therapeutic comparator. Based on studies that assessed the distribution of FITC-labeled BSA following oral gavage (Supplemental Fig. 2), AMT-101 administered by oral gavage in these studies probably had limited access to the colon and was likely delivered to a greater extent in small intestinal segments.

Despite this dosing limitation, treatment with AMT-101 (8.45 mg/kg) and 5-ASA showed statistically significant improvements in colon weight/length ratio (27%) and histopathology severity score (36%) that were comparable to 5-ASA–treated animals; effects on colon weight (Fig. 8A) and histology scores tabulated by a veterinary pathologist who was blinded to treatment groups (Fig. 8B) are shown. Compared with vehicle-treated animals, nonstatistically significant improvements for AMT-101 treatment was observed for body weight (Supplemental Fig. 6A) and survival (Supplemental Fig. 6B), as well as hemoccult positivity, stool consistency, and disease activity index (Supplemental Fig. 6C). In general, AMT-101 showed improvements that were comparable to the positive control (5-ASA). At study termination, micrographs of isolated distal colonic tissues showed that AMT-101 substantially protected colonic tissue from pathological modifications induced by Oxa (Fig. 8B, 8C).

To further examine the potential for AMT-101 to rectify pathological changes induced in models of induced colitis, we analyzed a panel of plasma chemokines, growth factors, and cytokines associated with inflammation. Of note, Oxa-induced changes in IL-6, G-CSF/CSF3, IL-28, IL-10, and IL-17A were prevented by AMT-101 treatment (Fig. 8D). Increased plasma levels of IL-4, IL-5, and IL-13 were also suppressed by AMT-101 (Fig. 8E). We also observed AMT-101 treatment–mediated suppression of increased plasma levels of M-CSF 1, IL-12 p70 protein, and IL-3 (Supplemental Fig. 6D), as well as LPS-inducible CXC chemokine (LIX), LIF, MIP1-α (CCL3), MIP-1β (CCL4), monocyte-chemotactic protein 3 (MCP3; CCL7), and IFN-γ–induced protein 10 (IP10; CXCL10) levels that had been induced by Oxa (Fig. 8A). Similar to these chemokines, increases in circulating levels of vascular endothelial growth factor and the IL-15/IL-15R complex were also rectified (data not shown). Interestingly, corrections observed with AMT-101 for most of these chemokines, growth factors, and cytokines did not occur in the 5-ASA treatment group, suggesting different mechanisms of action for AMT-101 and 5-ASA in suppressing pathological aspects of Oxa-induced colitis in mice. The observation that plasma levels of endogenous (mouse) IL-10 was increased in this Oxa-induced colitis model suggests that these animals actively tried to repress the upregulated proinflammatory mechanism(s). Notably, AMT-101 rectified this increase in mouse IL-10 secretion either directly by signaling that insufficient IL-10 was no longer an issue or indirectly as a result of AMT-101 rectification of upregulated proinflammatory mechanism(s). Finally, plasma IL-1Ra levels in mice with Oxa-induced colitis were observed to increase in an AMT-101 dose-dependent manner (Fig. 8F). At the highest dosage tested by oral gavage

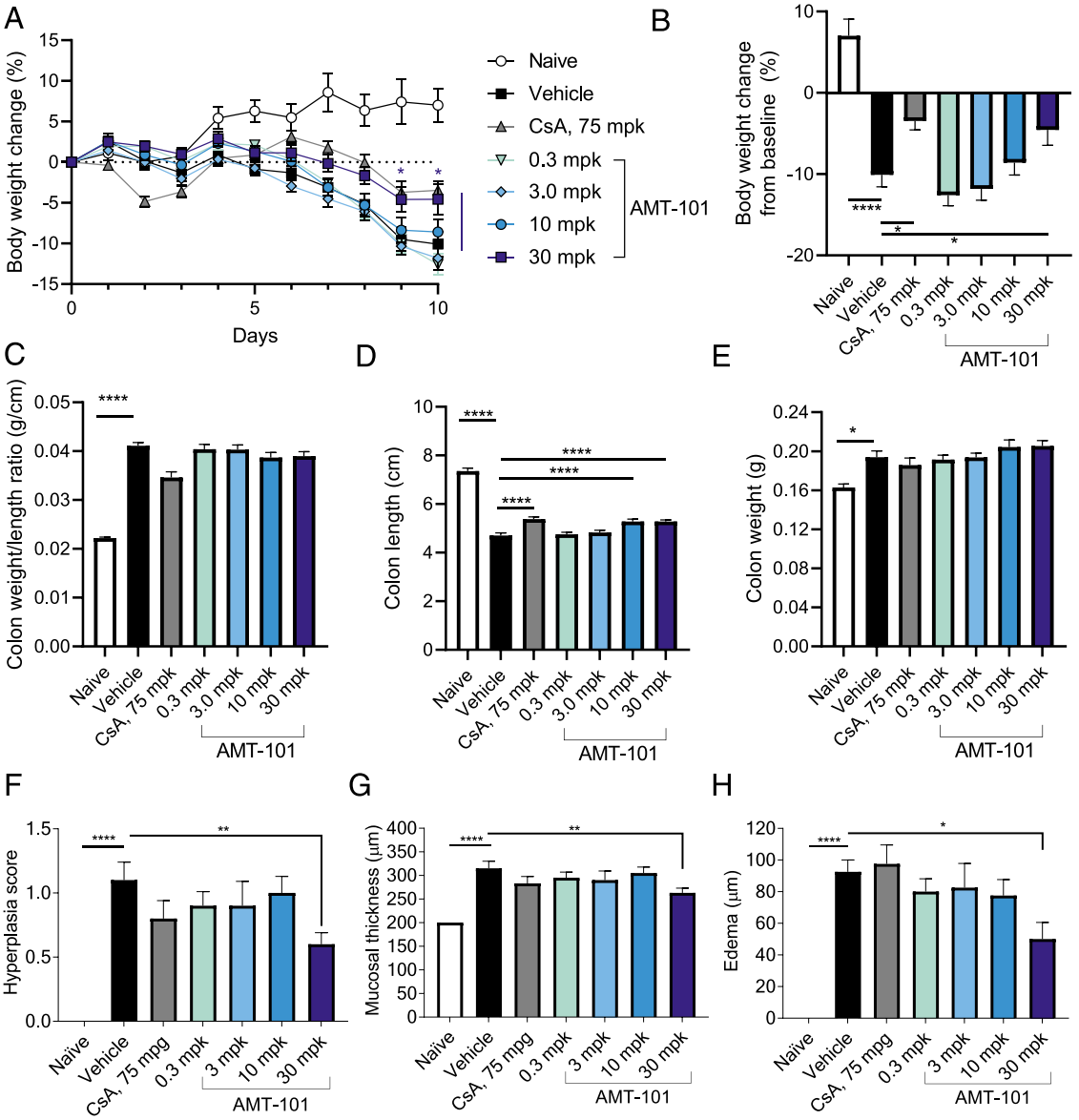

FIGURE 7. AMT-101 suppression of colitis-like symptoms in mice induced by DSS. (**A**) Daily body weights during the in-life portion of the study and (**B**) changes in body weight at study termination. (**C**) Colon weight to length ratio, (**D**) colon length, and (**E**) colon weight at study termination. AMT-101 reduces colon hyperplasia, mucosal thickness, and edema outcomes in DSS-induced colitis model. Individual score parameters for mice with DSS-induced colitis of (**F**) hyperplasia, (**G**) mucosal thickness, and (**H**) edema in the middle colonic tissues isolated at study termination. $n = 5$ naive, and $n = 10$ all other groups. Mean ± SEM. $*p < 0.05$, $**p < 0.01$, $****p < 0.0001$, differences versus vehicle assessed by two-way ANOVA with Dunnett analysis.

(9 mg/kg), we observed not only an increase in intestinal tissue IL-1Ra RNA levels but also a suppression in the increased IL-1β RNA levels (Fig. 8G). The ratio of IL-1Ra/IL-1β, used as an index of inflammation in a number of heredity autoimmune diseases (34), was strikingly shifted to a noninflamed balance point.

Discussion

In these studies, we have described a strategy to overcome the challenge of locally administering IL-10 to the intestinal lamina propria without significant systemic exposure, providing, to our knowledge, a novel approach to control inflammation associated with IBD pathogenesis (35, 36). To achieve this outcome, we employed a fragment (Chx386) of the Chx protein, a virulence factor secreted by nonpandemic strains of the human intestinal pathogen *Vibrio cholerae* (37–39). Previously, carrier elements of Chx were demonstrated to rapidly and efficiently ferry a nonChx biopharmaceutical cargo (human growth hormone [hGH]) across intestinal epithelia in vitro and in vivo through a process that hijacked an endogenous trafficking pathway that avoids lysosomal degradation (19). In the case of Chx-hGH, a single Chx carrier was used to transport a single hGH molecule. In this study, a similar genetic construction strategy was used to generate Chx–hIL-10, but because of the dimerization of hIL-10, AMT-101 was composed of two Chx carrier elements attached to a single hIL-10 dimer. The comparable transcytosis capabilities of Chx-hGH (19) and AMT-101 (this study) demonstrates that the trafficking pathway hijacked by Chx can accommodate single or double formats of the carrier. That transcytosis rates for AMT-101 (~125 kDa) and Chx-hGH (~50 kDa) were very similar in both instances is consistent with a vesicular transport process used by Chx.

Multiple in vitro analyses were performed to ensure that the spatial organization of AMT-101 accommodated the functional requirements of both the hIL-10 and the Chx386 carrier components. Although studies of hIL-10R binding and signaling

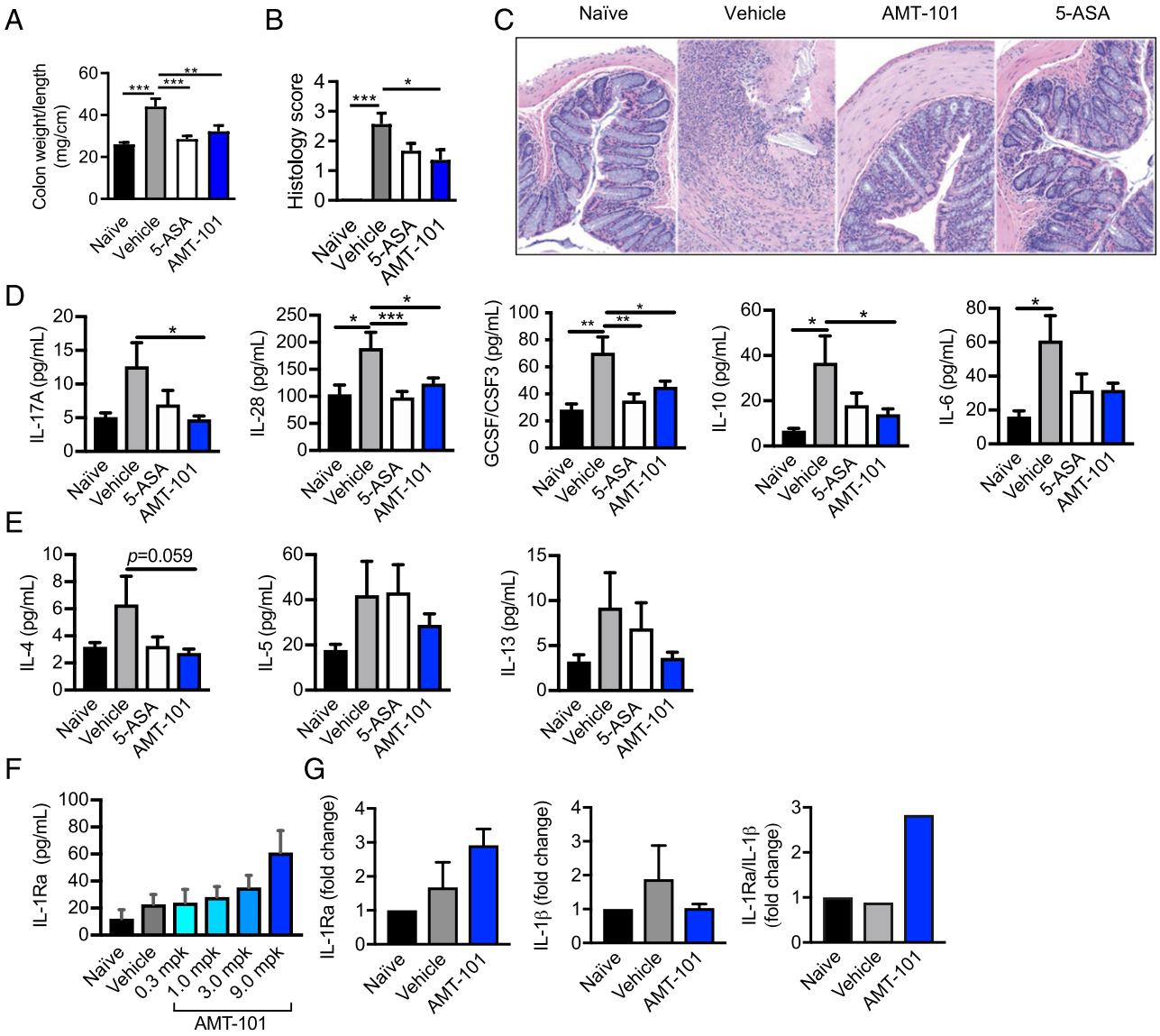

FIGURE 8. Prophylactic AMT-101 blocks Oxa-induced colitis in mice. (**A**) AMT-101 (9 mg/kg [mpk], oral gavage) reduces colon weight/length and (**B**) distal colon histopathology scoring of (**C**) distal colon sectioned micrographs; original magnification ×10. (**D**) AMT-101 (9 mpk) decreases plasma IL-17A, IL-28, G-CSF/CSF3, IL-10, IL-6 (**E**), IL-4, IL-5, and IL-13 (**F**) and increases plasma IL-1Ra (E) and the (**G**) colon IL-1Ra/IL-1b gene. Histopathology scores are based on board-certified veterinarian pathologist evaluation and include level of inflammation, level of leukocytic infiltration, transmural infiltration, loss of goblet cells, high vascular density, inflammation, and thickening of colon wall and/or ulceration. (A, B, C, F, and G) Naive (n = 5), vehicle (n = 7), 5-ASA (n = 11), and AMT-101 (n = 12). (D and E) Data of two studies combined and include naive (n = 10), vehicle (n = 14), 5-ASA (100 mpk; n = 22), and AMT-101 (n = 22). Mean + SEM. *$p < 0.05$, **$p < 0.01$, ***$p < 0.001$, by one-way ANOVA, multiple Dunnett comparisons test as compared with vehicle.

demonstrated AMT-101 (~125 kDa) to be less active in vitro than a commercial preparation of hIL-10 (~18 kDa), such differences likely reflect receptor binding actions of Chx386. In vivo studies, however, showed that such differences were not important as a commercial preparation of hIL-10 failed to effectively reach the underlying lamina propria following luminal application to the intestinal mucosa, whereas AMT-101 was able to effectively induce receptor-mediated IL-10 signaling (evidenced by increased pSTAT3) in cells within the lamina propria. This latter point highlights the fact that AMT-101, following in vivo transcytosis, retains a functional hIL-10 component. Following transcytosis, the Chx386 element of AMT-101 appears to limit the systemic distribution of hIL-10 activity through its sequestration by $CD3^+$ cells within the lamina propria. Retention of AMT-101 within the lamina propria was a design feature of this fusion protein strategy, with the uncertainty being if Chx-based sequestration into $CD3^+$ cells would outcompete the ability of the hIL-10 element to act on its cognate receptors within this compartment. Differences in systemic exposure in healthy versus diseased mice may be attributed to increased intestinal retention due to a higher number of infiltrating lamina propria immune cells in the disease state to which AMT-101 can target. Based upon the low doses required for maximum activity, our data demonstrate effective IL-10R activation occurring prior to local clearance through the Chx386 component of AMT-101.

Our observation that luminal introduction of commercial hIL-10 could induce pSTAT3 in some enterocytes was consistent with previous findings that the IL-10R is present at the apical surface of mouse intestinal epithelia (25). It is interesting to note, however, that we failed to observe pSTAT3 activation within the lamina propria for commercial hIL-10 dosed by ILI; such outcomes are consistent with the lack of clinical progression for efforts to use

transgenic bacteria expressing hIL-10 in the intestinal lumen as a way to deliver this cytokine to the lamina propria (30). Interestingly, we failed to observe pSTAT3 induction in enterocytes following the luminal introduction of AMT-101, suggesting that AMT-101 endocytosis is either too rapid to allow for IL-10R activation at the luminal epithelial surface and/or that organization of the AMT-101 elements somehow limits its access to IL-10R proteins at the luminal plasma membrane. Following A→B transcytosis, AMT-101induced pSTAT3 primarily in macrophage cells within the lamina propria but also in $CD3^+$ cells located within the lamina propria and at locations consistent with the distribution of intraepithelial lymphocytes. Both intraepithelial lymphocytes and macrophages are pivotal players in the production of chemokines, growth factors, and cytokines associated with both anti- and proinflammatory events and could have accounted for the changes observed in plasma cytokine profiles observed with AMT-101 treatment.

The potential for cells within the lamina propria to secrete anti- and proinflammatory agents in response to AMT-101 presents an interesting perspective for the efficacy outcomes observed in the DSS and Oxa models of induced colitis in which mice received AMT-101 by oral gavage. Based upon visual imaging of fluorescent protein distribution and AMT-101 tissue content measurements following oral gavage, it appears that only a fraction of the administered dose likely reached the colon, yet effects on pathological parameters of the colon were demonstrated. This suggests that events occurring at sites of AMT-101 uptake somehow resulted in panintestinal actions. In the case of induced mouse models of colitis, we observed a suppression of agents known to be associated with the inflammatory state of intestinal tissue. When AMT-101 was dosed in healthy animals, an induction of the anti-inflammatory protein IL-1Ra was observed. These observations suggest therapeutic benefit from the oral administration of AMT-101 may not require directed targeting to sites of inflammation but that a general resetting of the inflammatory state of the intestine may occur. Thus, the approach described in these studies to target hIL-10 delivery to the intestinal lamina propria provides support for the concept that local events within this compartment can also impact regulators of systemic inflammation (40).

IL-1Ra is a bona fide downstream target of IL-10, which can restore intestinal health by suppressing activity of the proinflammatory cytokine IL-1β (41). Further, the IL-1Ra/IL-1β ratio inversely correlates with IBD severity (30). Thus, modulation of the IL-Ra/IL-1β ratio by AMT-101 could provide a therapeutically relevant clinical index for AMT-101 actions. Oral gavage of AMT-101 in healthy mice resulted in a dose-dependent increase in plasma levels of IL-1Ra as well as an increase in the ratio of IL-1Ra/IL-1β gene expression. Pancolonic exposure of AMT-101 in noninflamed NHPs at relatively low levels (1–10 mg) also demonstrated an increase in plasma IL-1Ra levels that correlated with pSTAT3 induction in the absence of appreciable AMT-101 plasma levels. Thus, AMT-101 dosed in this way points toward a total dose in range of 10 mg or less to potentially provide maximum pharmacodynamics without detectable plasma pharmacokinetics (PK) to achieve the desired pharmacological intestinal actions of IL-10 with a minimized systemic exposure profile.

In sum, our studies have described a method to deliver biologically active hIL-10 to the intestinal lamina propria that results in minimal systemic PK while allowing full pharmacodynamics associated with this potent anti-inflammatory cytokine. AMT-101 was shown to efficiently and rapidly transport across intact intestinal epithelia to focus hIL-10 actions (via pSTAT3 activation) on macrophage cells and lymphocytes with ultimate sequestration by $CD3^+$ cells within the lamina propria to limit systemic exposure. Actions demonstrated for AMT-101 provide a means to directly test the hypothesis that the benefits of systemic rhIL-10 examined previously in the clinic to treat IBD patients were limited by toxicities resulting from systemic administration and not a lack of efficacy in these disease settings.

Acknowledgments

We thank Michael Zachariadis (University of Bath microscopy suite) as well as Martin Bradshaw and Jane Graham (University of Bath Bioscience Services Unit) for support.

Disclosures

All Applied Molecular Transport employees hold stock in the company and stand to benefit financially from increases in the value of that stock. The other authors have no financial conflicts of interest.

References

1. Mocellin, S., F. Marincola, C. R. Rossi, D. Nitti, and M. Lise. 2004. The multifaceted relationship between IL-10 and adaptive immunity: putting together the pieces of a puzzle. *Cytokine Growth Factor Rev.* 15: 61–76.
2. Mosmann, T. R. 1994. Properties and functions of interleukin-10. *Adv. Immunol.* 56: 1–26.
3. Neumann, C., A. Scheffold, and S. Rutz. 2019. Functions and regulation of T cell-derived interleukin-10. *Semin. Immunol.* 44: 101344.
4. Paul, G., V. Khare, and C. Gasche. 2012. Inflamed gut mucosa: downstream of interleukin-10. *Eur. J. Clin. Invest.* 42: 95–109.
5. Glocker, E. O., D. Kotlarz, C. Klein, N. Shah, and B. Grimbacher. 2011. IL-10 and IL-10 receptor defects in humans. *Ann. N. Y. Acad. Sci.* 1246: 102–107.
6. Lin, Z., Z. Wang, J. P. Hegarty, T. R. Lin, Y. Wang, S. Deiling, R. Wu, N. J. Thomas, and J. Floros. 2017. Genetic association and epistatic interaction of the interleukin-10 signaling pathway in pediatric inflammatory bowel disease. *World J. Gastroenterol.* 23: 4897–4909.
7. Aithal, G. P., A. Craggs, C. P. Day, M. Welfare, A. K. Daly, J. C. Mansfield, and M. Hudson. 2001. Role of polymorphisms in the interleukin-10 gene in determining disease susceptibility and phenotype in inflamatory bowel disease. *Dig. Dis. Sci.* 46: 1520–1525.
8. Amre, D. K., D. R. Mack, K. Morgan, D. Israel, P. Lambrette, I. Costea, A. Krupoves, H. Fegury, J. Dong, G. Grimard, et al. 2009. Interleukin 10 (IL-10) gene variants and susceptibility for paediatric onset Crohn's disease. *Aliment. Pharmacol. Ther.* 29: 1025–1031.
9. Wang, A. H., W. J. Lam, D. Y. Han, Y. Ding, R. Hu, A. G. Fraser, L. R. Ferguson, and A. R. Morgan. 2011. The effect of IL-10 genetic variation and interleukin 10 serum levels on Crohn's disease susceptibility in a New Zealand population. *Hum. Immunol.* 72: 431–435.
10. Quiros, M., H. Nishio, P. A. Neumann, D. Siuda, J. C. Brazil, V. Azcutia, R. Hilgarth, M. N. O'Leary, V. Garcia-Hernandez, G. Leoni, et al. 2017. Macrophage-derived IL-10 mediates mucosal repair by epithelial WISP-1 signaling. *J. Clin. Invest.* 127: 3510–3520.
11. Shouval, D. S., A. Biswas, J. A. Goettel, K. McCann, E. Conaway, N. S. Redhu, I. D. Mascanfroni, Z. Al Adham, S. Lavoie, M. Ibourk, et al. 2014. Interleukin-10 receptor signaling in innate immune cells regulates mucosal immune tolerance and anti-inflammatory macrophage function. *Immunity* 40: 706–719.
12. Colombel, J. F., P. Rutgeerts, H. Malchow, M. Jacyna, O. H. Nielsen, J. Rask-Madsen, S. Van Deventer, A. Ferguson, P. Desreumaux, A. Forbes, et al. 2001. Interleukin 10 (Tenovil) in the prevention of postoperative recurrence of Crohn's disease. *Gut* 49: 42–46.
13. Fedorak, R. N., A. Gangl, C. O. Elson, P. Rutgeerts, S. Schreiber, G. Wild, S. B. Hanauer, A. Kilian, M. Cohard, A. LeBeaut, and B. Feagan. 2000. Recombinant human interleukin 10 in the treatment of patients with mild to moderately active Crohn's disease. The interleukin 10 inflammatory bowel disease cooperative study group. *Gastroenterology* 119: 1473–1482.
14. Schreiber, S., R. N. Fedorak, O. H. Nielsen, G. Wild, C. N. Williams, S. Nikolaus, M. Jacyna, B. A. Lashner, A. Gangl, P. Rutgeerts, et al. 2000. Safety and efficacy of recombinant human interleukin 10 in chronic active Crohn's disease. Crohn's disease IL-10 cooperative study group. *Gastroenterology* 119: 1461–1472.
15. Marlow, G. J., D. van Gent, and L. R. Ferguson. 2013. Why interleukin-10 supplementation does not work in Crohn's disease patients. *World J. Gastroenterol.* 19: 3931–3941.
16. Olszak, T., J. F. Neves, C. M. Dowds, K. Baker, J. Glickman, N. O. Davidson, C. S. Lin, C. Jobin, S. Brand, K. Sotlar, et al. 2014. Protective mucosal immunity mediated by epithelial CD1d and IL-10. *Nature* 509: 497–502.
17. Jørgensen, R., A. E. Purdy, R. J. Fieldhouse, M. S. Kimber, D. H. Bartlett, and A. R. Merrill. 2008. Cholix toxin, a novel ADP-ribosylating factor from *Vibrio cholerae*. *J. Biol. Chem.* 283: 10671–10678.
18. Simon, N. C., K. Aktories, and J. T. Barbieri. 2014. Novel bacterial ADP-ribosylating toxins: structure and function. *Nat. Rev. Microbiol.* 12: 599–611.
19. Taverner, A., J. MacKay, F. Laurent, T. Hunter, K. Liu, K. Mangat, L. Song, E. Seto, S. Postlethwaite, A. Alam, et al. 2020. Cholix protein domain I functions

as a carrier element for efficient apical to basal epithelial transcytosis. *Tissue Barriers* 8: 1710429.
20. Chen, X., Y. Bai, J. L. Zaro, and W. C. Shen. 2010. Design of an in vivo cleavable disulfide linker in recombinant fusion proteins. *Biotechniques* 49: 513–518.
21. Yoon, S. I., N. J. Logsdon, F. Sheikh, R. P. Donnelly, and M. R. Walter. 2006. Conformational changes mediate interleukin-10 receptor 2 (IL-10R2) binding to IL-10 and assembly of the signaling complex. *J. Biol. Chem.* 281: 35088–35096.
22. Zdanov, A., C. Schalk-Hihi, A. Gustchina, M. Tsang, J. Weatherbee, and A. Wlodawer. 1995. Crystal structure of interleukin-10 reveals the functional dimer with an unexpected topological similarity to interferon gamma. *Structure* 3: 591–601.
23. Korz, D. J., U. Rinas, K. Hellmuth, E. A. Sanders, and W. D. Deckwer. 1995. Simple fed-batch technique for high cell density cultivation of *Escherichia coli*. *J. Biotechnol.* 39: 59–65.
24. Syto, R., N. J. Murgolo, E. H. Braswell, P. Mui, E. Huang, and W. T. Windsor. 1998. Structural and biological stability of the human interleukin 10 homodimer. *Biochemistry* 37: 16943–16951.
25. Lanis, J. M., E. E. Alexeev, V. F. Curtis, D. A. Kitzenberg, D. J. Kao, K. D. Battista, M. E. Gerich, L. E. Glover, D. J. Kominsky, and S. P. Colgan. 2017. Tryptophan metabolite activation of the aryl hydrocarbon receptor regulates IL-10 receptor expression on intestinal epithelia. *Mucosal Immunol.* 10: 1133–1144.
26. Ostanin, D. V., J. Bao, I. Koboziev, L. Gray, S. A. Robinson-Jackson, M. Kosloski-Davidson, V. H. Price, and M. B. Grisham. 2009. T cell transfer model of chronic colitis: concepts, considerations, and tricks of the trade. *Am. J. Physiol. Gastrointest. Liver Physiol.* 296: G135–G146.
27. Dinarello, C. A. 2018. Overview of the IL-1 family in innate inflammation and acquired immunity. *Immunol. Rev.* 281: 8–27.
28. Jenkins, J. K., M. Malyak, and W. P. Arend. 1994. The effects of interleukin-10 on interleukin-1 receptor antagonist and interleukin-1 beta production in human monocytes and neutrophils. *Lymphokine Cytokine Res.* 13: 47–54.
29. Soendergaard, C., O. H. Nielsen, J. B. Seidelin, P. H. Kvist, and J. T. Bjerrum. 2015. Alpha-1 antitrypsin and granulocyte colony-stimulating factor as serum biomarkers of disease severity in ulcerative colitis. *Inflamm. Bowel Dis.* 21: 1077–1088.
30. Dionne, S., I. D. D'Agata, J. Hiscott, T. Vanounou, and E. G. Seidman. 1998. Colonic explant production of IL-1and its receptor antagonist is imbalanced in inflammatory bowel disease (IBD). *Clin. Exp. Immunol.* 112: 435–442.
31. Schülke, S. 2018. Induction of interleukin-10 producing dendritic cells as a tool to suppress allergen-specific T helper 2 responses. *Front. Immunol.* 9: 455.
32. Laroui, H., S. A. Ingersoll, H. C. Liu, M. T. Baker, S. Ayyadurai, M. A. Charania, F. Laroui, Y. Yan, S. V. Sitaraman, and D. Merlin. 2012. Dextran sodium sulfate (DSS) induces colitis in mice by forming nano-lipocomplexes with medium-chain-length fatty acids in the colon. *PLoS One* 7: e32084.
33. Randhawa, P. K., K. Singh, N. Singh, and A. S. Jaggi. 2014. A review on chemical-induced inflammatory bowel disease models in rodents. *Korean J. Physiol. Pharmacol.* 18: 279–288.
34. Dayer, J. M., F. Oliviero, and L. Punzi. 2017. A brief history of IL-1 and IL-1 Ra in rheumatology. *Front. Pharmacol.* 8: 293.
35. Chen, M. L., and M. S. Sundrud. 2016. Cytokine networks and T-cell subsets in inflammatory bowel diseases. *Inflamm. Bowel Dis.* 22: 1157–1167.
36. Neurath, M. F. 2014. Cytokines in inflammatory bowel disease. *Nat. Rev. Immunol.* 14: 329–342.
37. Awasthi, S. P., M. Asakura, N. Chowdhury, S. B. Neogi, A. Hinenoya, H. M. Golbar, J. Yamate, E. Arakawa, T. Tada, T. Ramamurthy, and S. Yamasaki. 2013. Novel cholix toxin variants, ADP-ribosylating toxins in *Vibrio cholerae* non-O1/non-O139 strains, and their pathogenicity. *Infect. Immun.* 81: 531–541.
38. Chen, Y., J. A. Johnson, G. D. Pusch, J. G. Morris, Jr., and O. C. Stine. 2007. The genome of non-O1 *Vibrio cholerae* NRT36S demonstrates the presence of pathogenic mechanisms that are distinct from those of O1 *Vibrio cholerae*. *Infect. Immun.* 75: 2645–2647.
39. Purdy, A. E., D. Balch, M. L. Lizárraga-Partida, M. S. Islam, J. Martinez-Urtaza, A. Huq, R. R. Colwell, and D. H. Bartlett. 2010. Diversity and distribution of cholix toxin, a novel ADP-ribosylating factor from *Vibrio cholerae*. *Environ. Microbiol. Rep.* 2: 198–207.
40. Kverka, M., and H. Tlaskalova-Hogenova. 2013. Two faces of microbiota in inflammatory and autoimmune diseases: triggers and drugs. *APMIS* 121: 403–421.
41. Schreiber, S., T. Heinig, H. G. Thiele, and A. Raedler. 1995. Immunoregulatory role of interleukin 10 in patients with inflammatory bowel disease. *Gastroenterology* 108: 1434–1444.